

Supporting Information for

Structural, Optical and Magnetic Investigations in Lanthanide complexes Involving Multichelating TTF-based Ligands.

Saskia Speed,^a Min Feng,^a Guglielmo Fernandez Garcia,^{a,c} Fabrice Pointillart,^{*a} Bertrand Lefeuvre,^a François Riobé,^b Stéphane Golhen,^a Boris Le Guennic,^{*a} Federico Totti,^c Yannick Guyot,^d Olivier Cador,^a Olivier Maury,^b Lahcène Ouahab^a

^a Institut des Sciences Chimiques de Rennes UMR 6226 CNRS-UR1, Université de Rennes 1, 35042 Rennes Cedex, France

^b Univ Lyon, ENS de Lyon, CNRS UMR 5182, Université Claude Bernard Lyon 1, Laboratoire de Chimie, F69342, Lyon, France.

^c Dipartimento di Chimica, Università di Firenze, Via della Lastruccia 3 Polo Scientifico, 50019 Sesto Fiorentino, Italy.

^d Univ Lyon, Université Claude Bernard Lyon 1, CNRS UMR 5306, Institut Lumière Matière, 69622 Villeurbanne, France.

fabrice.pointillart@univ-rennes1.fr; boris.leguennic@univ-rennes1.fr

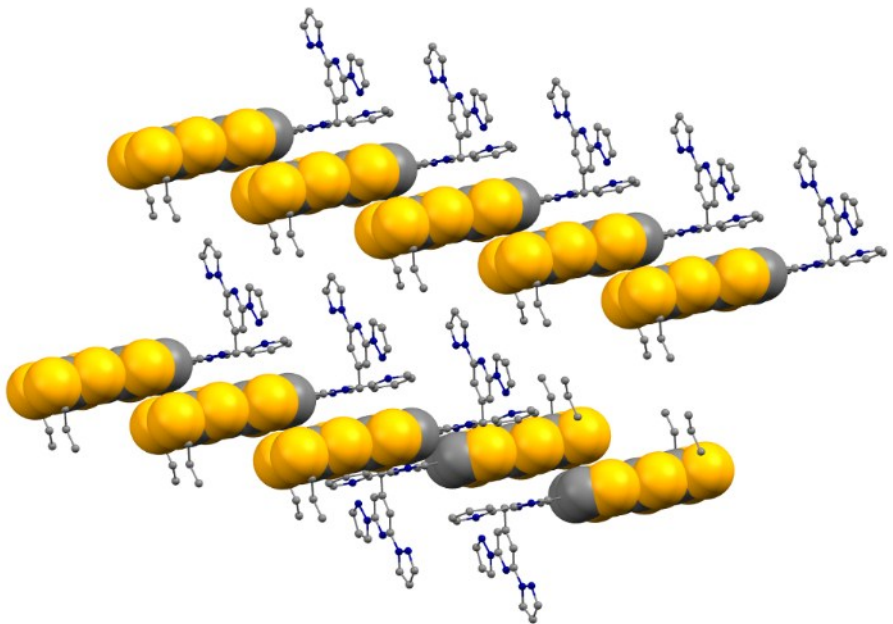


Figure S1. Crystal packing of \mathbf{L}^1 highlighting the formation of organic (spacefilling) and metallo-organic (ball and stick) networks.

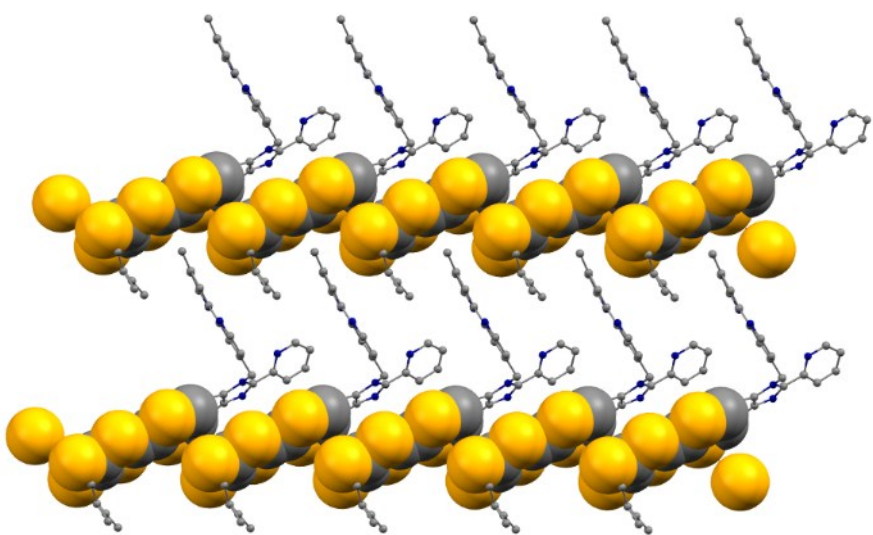


Figure S2. Crystal packing of \mathbf{L}^2 highlighting the formation of organic (spacefilling) and metallo-organic (ball and stick) networks.

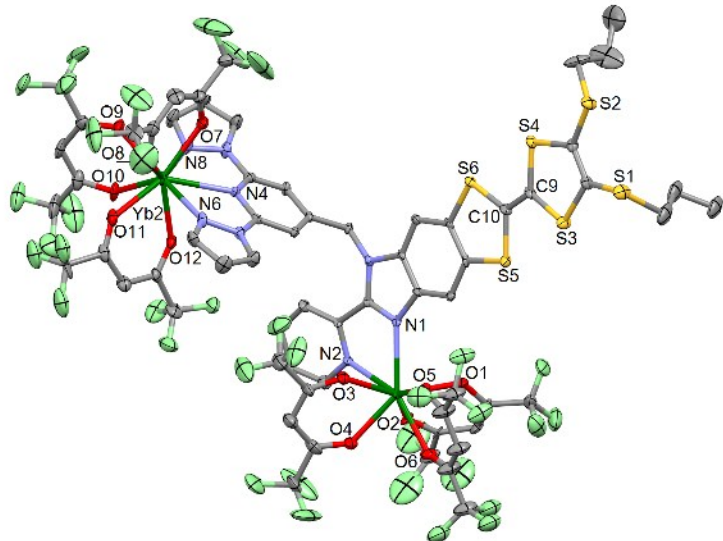


Figure S3. ORTEP view of **1**. Thermal ellipsoids are drawn at 30% probability. Hydrogen atoms and dichloromethane molecules of crystallization are omitted for clarity.

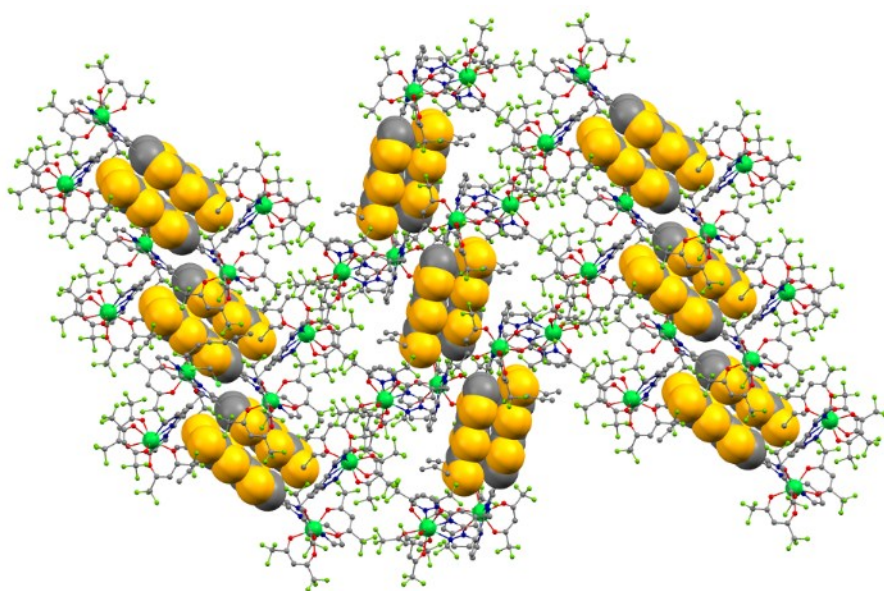


Figure S4. Crystal packing of **1** highlighting the formation of organic (spacefilling) and metallo-organic (ball and stick) networks.

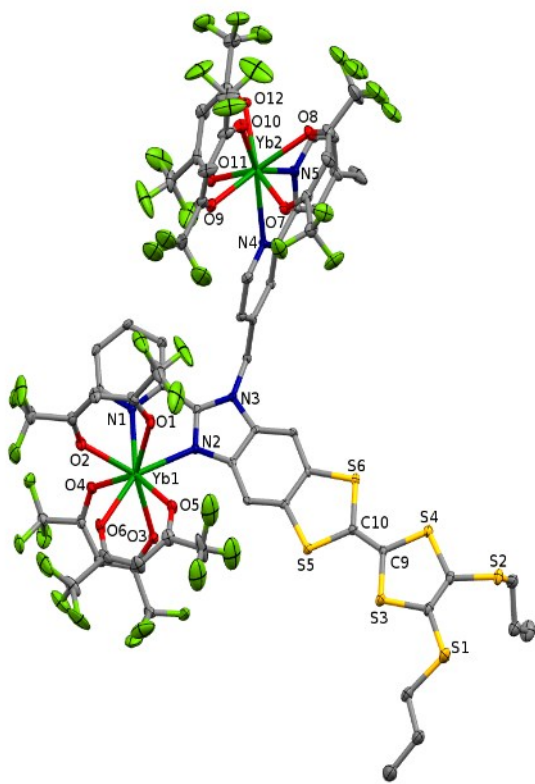


Figure S5. ORTEP view of **2**. Thermal ellipsoids are drawn at 30% probability. Hydrogen atoms and both dichloromethane and *n*-heptane molecules of crystallization are omitted for clarity.

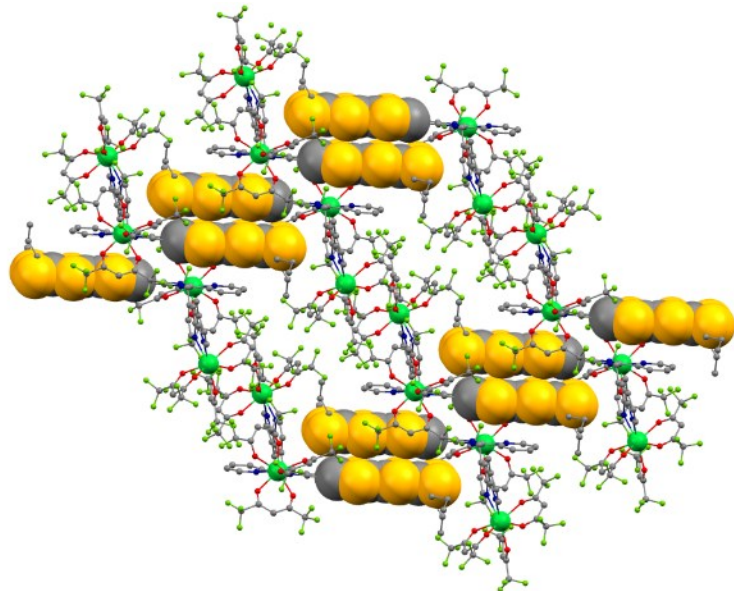


Figure S6. Crystal packing of **2** highlighting the formation of organic (spacefilling) and metallo-organic (ball and stick) networks.

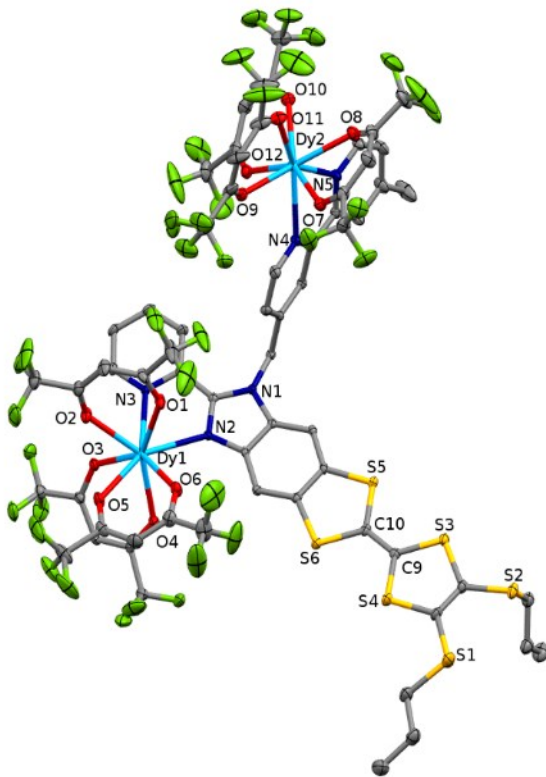


Figure S7. ORTEP view of **3**. Thermal ellipsoids are drawn at 30% probability. Hydrogen atoms and dichloromethane molecule are omitted for clarity.

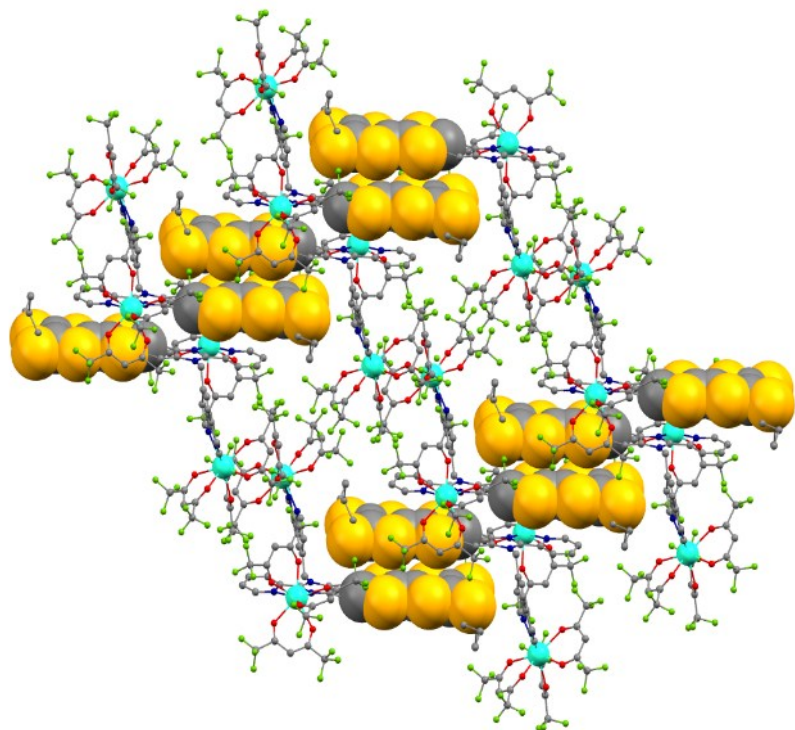


Figure S8. Crystal packing of **3** highlighting the formation of organic (spacefilling) and metallo-organic (ball and stick) networks.

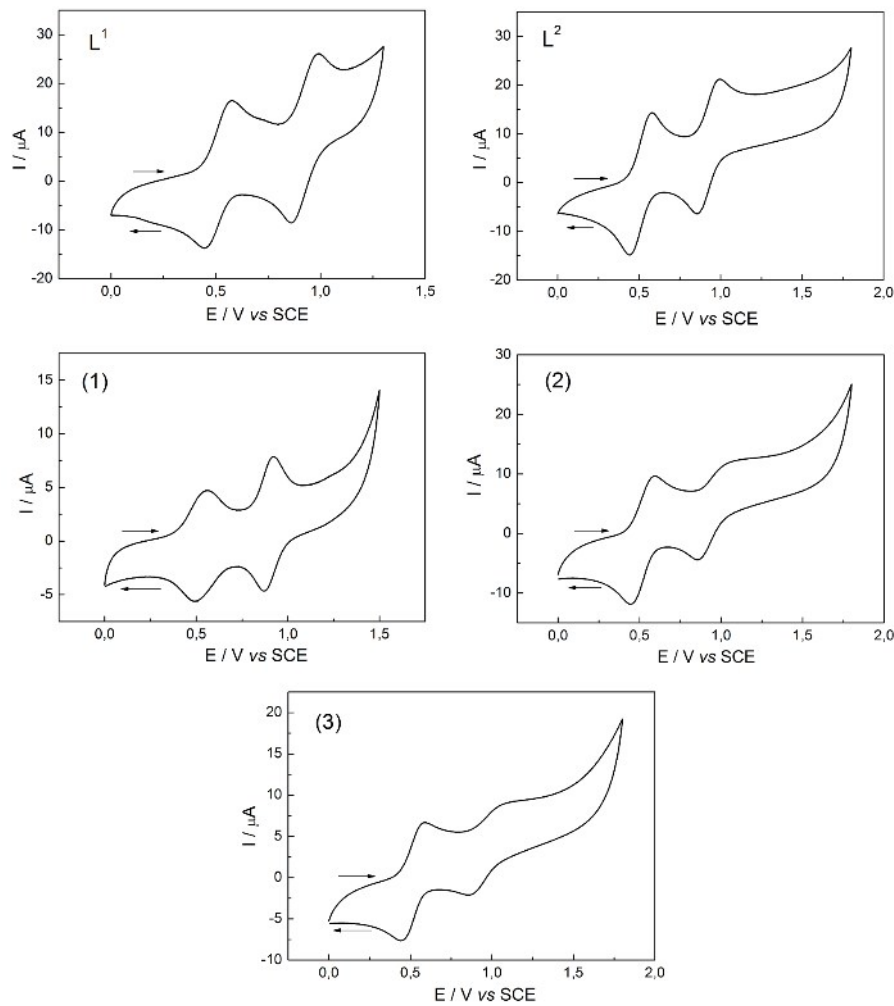


Figure S9. Cyclic voltammograms of **L¹**, **L²** and **1-3** in CH_2Cl_2 at a scan rate of $100 \text{ mV}\cdot\text{s}^{-1}$. The potentials were measured *vs.* a saturated calomel electrode (SCE) with Pt wires as working and counter electrodes.

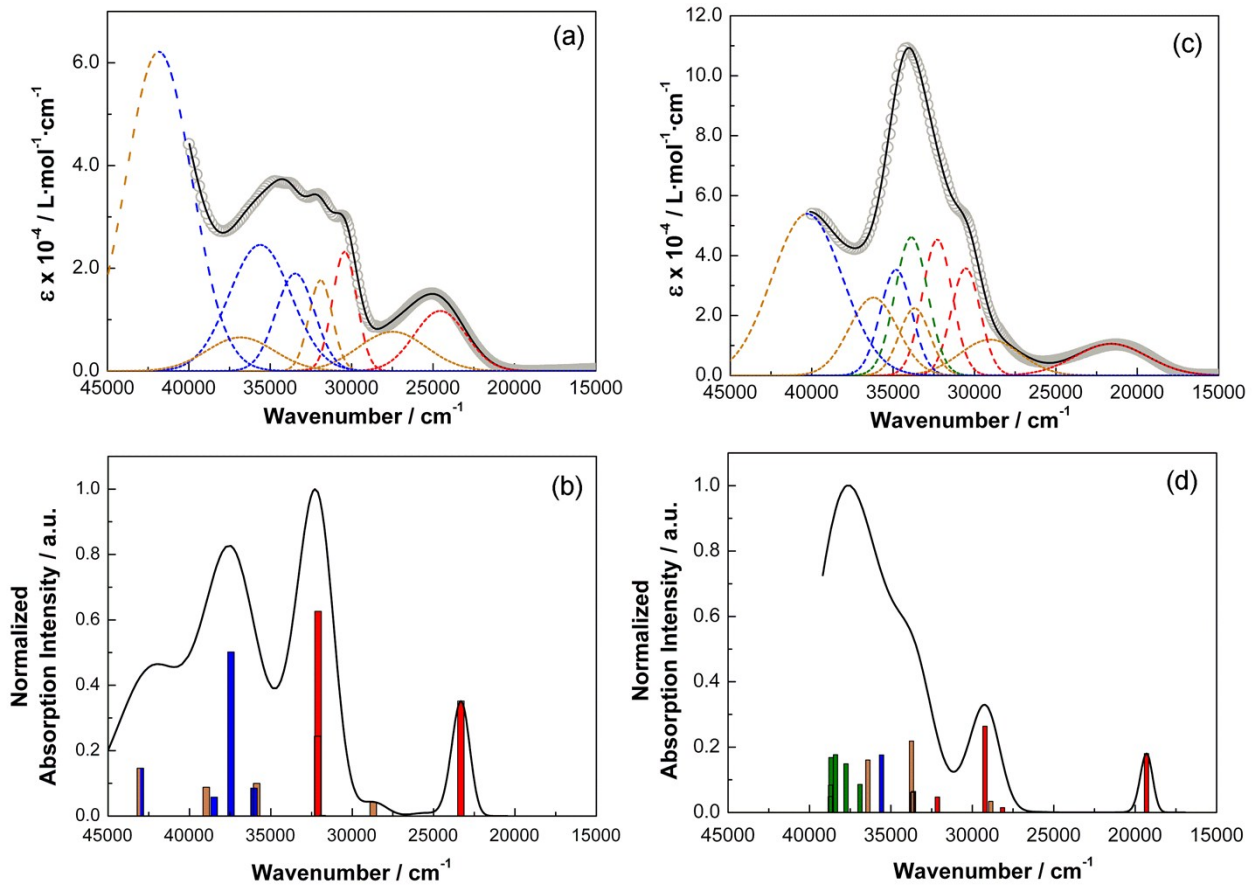


Figure S10. a) Experimental UV/vis absorption spectrum in solution ($c = 4 \cdot 10^{-5}$ M) of \mathbf{L}^2 in CH_2Cl_2 (open grey circles), respective Gaussian decompositions (dashed lines) and best fit (full black line). b) Theoretical absorption spectrum (black line), the bars represent the mean contribution of the absorption spectra that are listed in Table 6. c) Experimental UV/vis absorption spectrum in solution ($c = 4 \cdot 10^{-5}$ M) of $\mathbf{2}$ in CH_2Cl_2 (open grey circles), respective Gaussian decompositions (dashed lines) and best fit (full black line). d) Theoretical absorption spectrum (black line), the bars represent the mean contribution of the absorption spectra that are listed in Table 6.

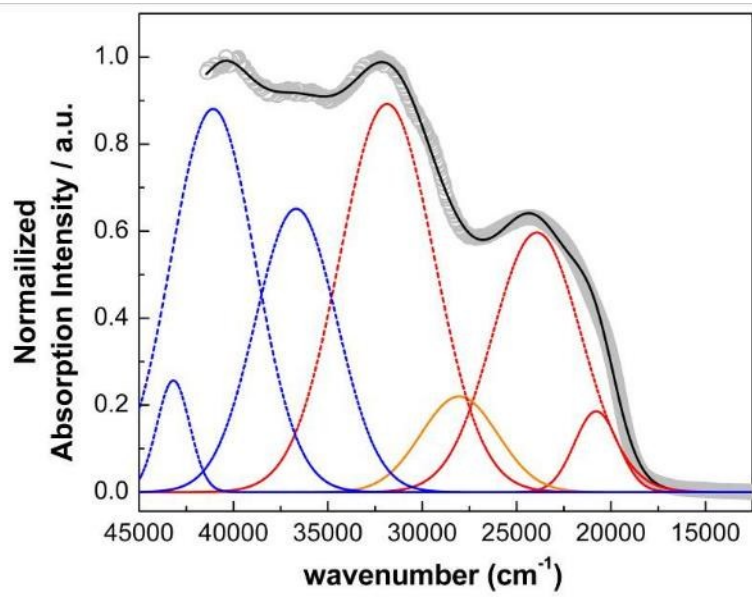


Figure S11. Experimental UV-visible absorption spectrum in solid-state (KBr pellets) of **L¹** (open gray circles). Gaussian decompositions (dashed lines) and best fit (full black line), R = 0.9993. The red, orange and blue dashed lines represent the intra-ligand charge transfer, intra-TTF, intra-acceptor absorption bands, respectively.

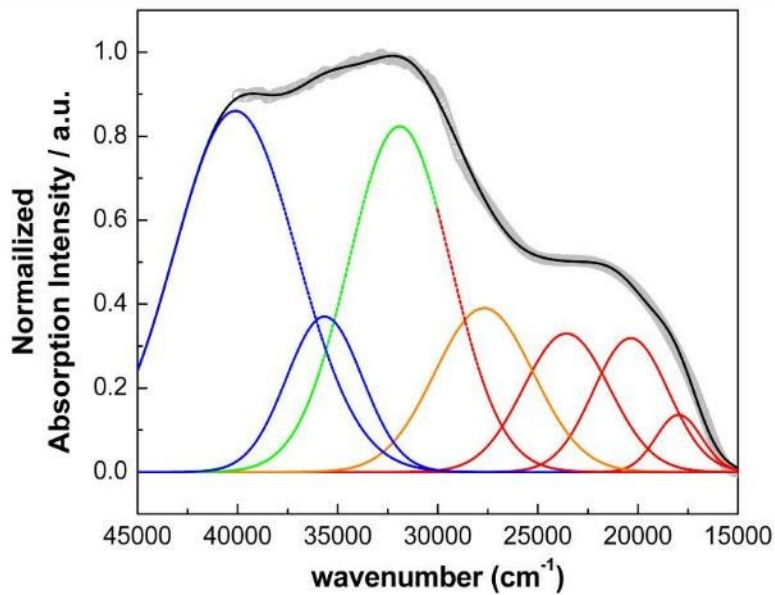


Figure S12. Experimental UV-visible absorption spectrum in solid-state (KBr pellets) of **1** (open gray circles). Gaussian decompositions (dashed lines) and best fit (full black line), R = 0.9993. The red, orange, green and blue dashed lines represent the intra-ligand charge transfer, intra-TTF, intra-hfac⁻ and intra-acceptor absorption bands, respectively.

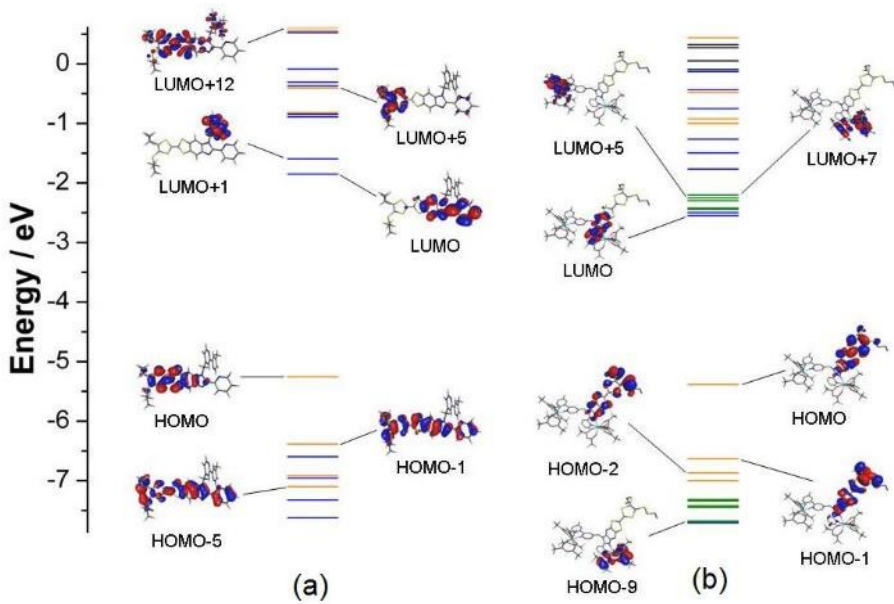


Figure S13. MO diagram of **L²** (left) and complex **2** (right). Energy levels of the centered TTF donor, dpp acceptor and hfac⁻ are represented in orange, blue and green, respectively.

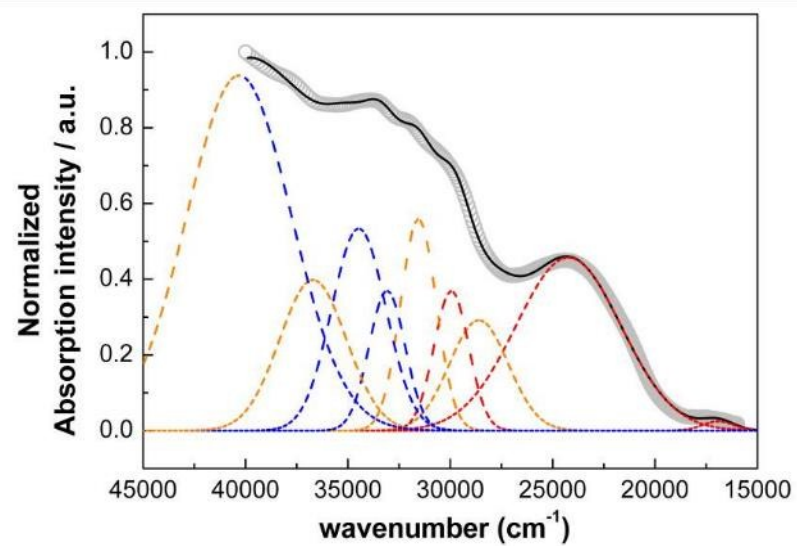


Figure S14. Experimental UV-visible absorption spectrum in solid-state (KBr pellets) of **L²** (open gray circles). Gaussian decompositions (dashed lines) and best fit (full black line), R = 0.9993. The red, orange and blue dashed lines represent the intra-ligand charge transfer, intra-TTF, intra-acceptor absorption bands, respectively.

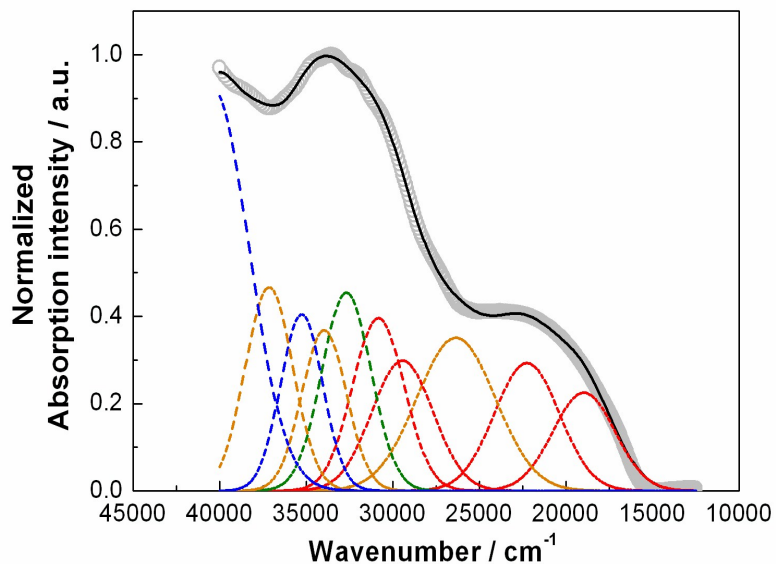


Figure S15. Experimental UV-visible absorption spectrum in solid-state (KBr pellets) of **3** (open gray circles). Gaussian decompositions (dashed lines) and best fit (full black line), $R = 0.9993$. The red, orange and blue dashed lines represent the intra-ligand charge transfer, intra-TTF, intra-acceptor absorption bands, respectively.

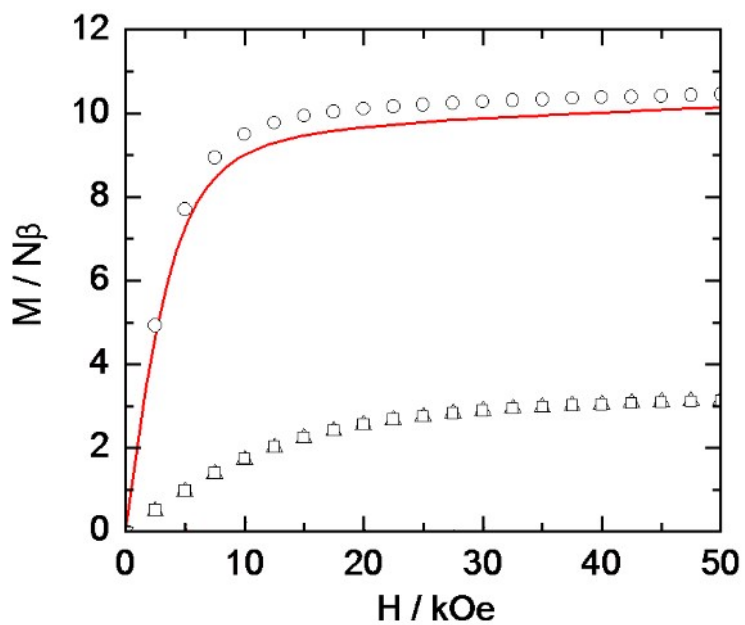


Figure S16. Magnetizations at 2 K for compounds **1** (triangles), **2** (squares) and **3** (circles) with simulated curve for **1** (full red line).

Extended Debye model:

$$\chi' = \chi_s + (\chi_t - \chi_s) \frac{1 + (\omega\tau)^{1-\alpha} \sin\left(\alpha \frac{\pi}{2}\right)}{1 + 2(\omega\tau)^{1-\alpha} \sin\left(\alpha \frac{\pi}{2}\right) + (\omega\tau)^{2-2\alpha}}$$

$$\chi'' = (\chi_t - \chi_s) \frac{(\omega\tau)^{1-\alpha} \cos\left(\alpha \frac{\pi}{2}\right)}{1 + 2(\omega\tau)^{1-\alpha} \sin\left(\alpha \frac{\pi}{2}\right) + (\omega\tau)^{2-2\alpha}}$$

With χ_t the isothermal susceptibility, χ_s the adiabatic susceptibility, τ the relaxation time and α the empiric parameter which describes the distribution of the relaxation time. For SMM with only one relaxing object α is close to zero. The extended Debye model was applied to fit simultaneously the experimental variations of χ_M' and χ_M'' with the frequency ν of the oscillating field ($\omega = 2\pi\nu$). The best fitted parameters τ , α , χ_t , χ_s (and the coefficient of determination R^2) are given in Figure S17 at 2 K and zero external dc field for compound 3.

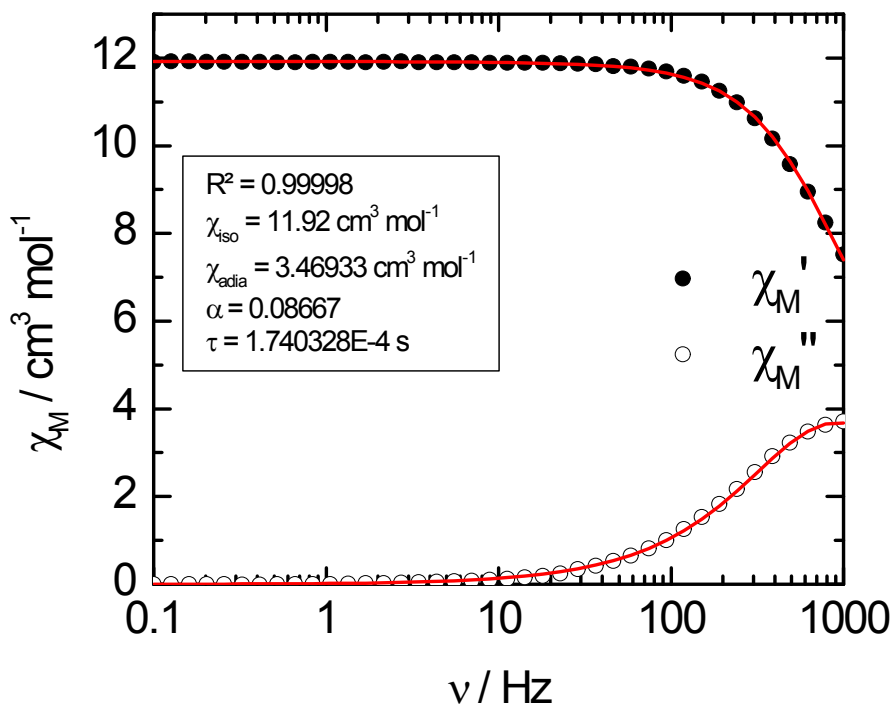


Figure S17. Frequency dependence of the ac susceptibility components χ_M' and χ_M'' at 2 K and in zero external dc field for compound 3 with the best fitted curve with extended Debye model.

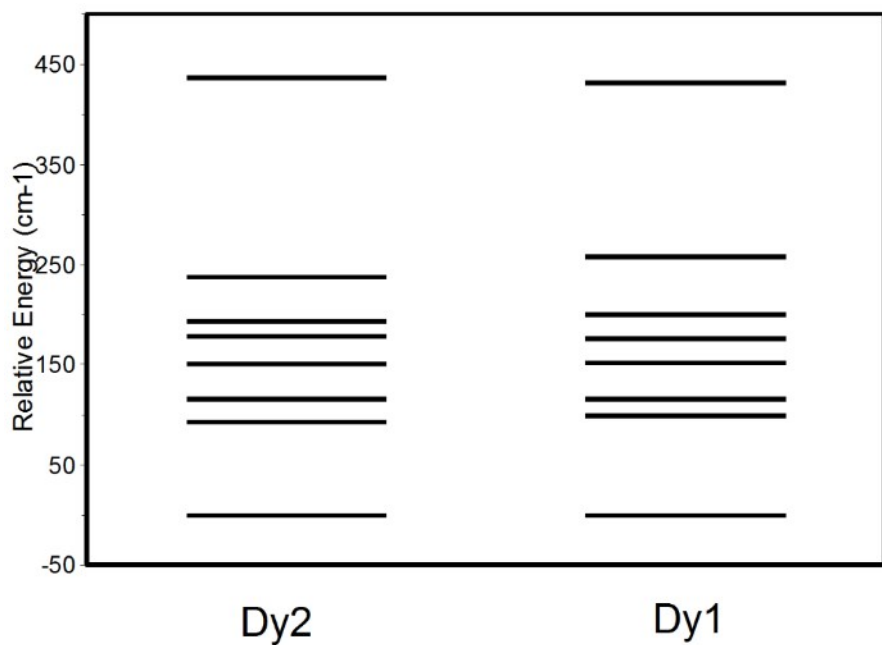


Figure S18. Energy splitting of the $^6\text{H}_{15/2}$ multiplet for Dy1 (on right) and Dy2 (on left).

Table S1. Selected bond lengths (\AA) for complexes **1-3**.

Compounds	1	2	3
Ln1-O1	2.283(10)	2.282(5)	2.320(4)
Ln1-O2	2.313(10)	2.318(5)	2.347(4)
Ln1-O3	2.291(11)	2.304(5)	2.344(4)
Ln1-O4	2.279(11)	2.306(5)	2.358(4)
Ln1-O5	2.305(10)	2.310(5)	2.330(4)
Ln1-O6	2.306(11)	2.292(5)	2.353(4)
Ln1-N1	2.455(11)	2.483(6)	/
Ln1-N2	2.533(12)	2.437(5)	2.496(4)
Ln1-N3	/	/	2.526(5)
Ln2-O7	2.344(12)	2.295(5)	2.334(4)
Ln2-O8	2.322(12)	2.299(5)	2.350(4)
Ln2-O9	2.267(11)	2.274(5)	2.314(4)
Ln2-O10	2.406(12)	2.291(5)	2.335(4)
Ln2-O11	2.294(12)	2.300(4)	2.321(4)
Ln2-O12	2.362(10)	2.280(5)	2.339(4)
Ln2-N4	2.556(11)	2.488(5)	2.529(4)
Ln2-N5	/	2.462(6)	2.517(5)
Ln2-N6	2.459(13)	/	/
Ln2-N8	2.452(13)	/	/

Table S2. SHAPE analysis of the coordination polyhedra around the lanthanide ions in complexes **1-3**.

	Metal	CShM _{SAPR-8} (square antiprism D _{4d})	CShM _{TDD-8} (triangular dodecahedron D _{2d})	CShM _{BTPR-8} (biaugmented trigonal prism C _{2v})	CShM _{TCTPR-9} (spherical tricapped trigonal prism D _{3h})	CShM _{CSAPR-9} (spherical capped square antiprism C _{4v})	CShM _{MFF-9} (Muffin C _s)
1	Yb1- N ₂ O ₆	0.380	2.768	2.298	-	-	-
	Yb2- N ₃ O ₆	-	-	-	0.554	0.949	1.293
2	Yb1- N ₂ O ₆	0.445	2.554	1.866	-	-	-
	Yb2- N ₂ O ₆	0.450	1.720	2.221	-	-	-
3	Dy1- N ₂ O ₆	0.631	2.572	1.762	-	-	-
	Dy2- N ₂ O ₆	0.530	1.644	2.142	-	-	-

Table S3. TD-DFT calculated excitation energies and main compositions of the low-lying electronic transitions for **L²** and **2**. In addition, the charge transfer and the pure intramolecular transitions are reported. ID, IA, H and L represent the intramolecular TTF (Donor) or intramolecular (Acceptor) transitions, and the HOMO and LUMO, respectively. Therefore, ILCT stands for Intra-Ligand Charge Transfer. The theoretical values are evaluated at the PCM(CH₂Cl₂)-PBE0/SVP level of approximation.

	E _{exp} (cm ⁻¹)	E _{theo} (cm ⁻¹)	Osc.	Type	Assignment	Transition
2	24500	23321	0.39	ILCT	$\pi_{\text{TTF}} \rightarrow \pi^*_{\text{bzip}}$	H→L (96%)
	27500	28703	0.05	ID	$\pi_{\text{TTF}} \rightarrow \pi^*_{\text{TTF}}$	H→L+5 (92%)
	30400	32101	0.27	ILCT	$\pi_{\text{TTF}} \rightarrow \pi^*_{\text{bzip}}$	H-1→L (83%)
		32124	0.05		$\pi_{\text{TTF}} \rightarrow \pi^*_{\text{Mebpy}}$	H→L+4 (75%)
	31900	33527	0.21	ID	$\pi_{\text{TTF}} \rightarrow \pi^*_{\text{TTF}}$	H-1→L+2 (13%) H→L+6 (56%)
	33400	35869	0.11	IA	$\pi_{\text{bzip}} \rightarrow \pi^*_{\text{Mebpy}}$	H-2→L+1 (83%)
		36041	0.10			
	35600	37453	0.56	IA	$\pi_{\text{Mebpy}} \rightarrow \pi^*_{\text{Mebpy}}$	H-4→L+1 (88%)
	36800	38482	0.06	ID	$\pi_{\text{TTF}} \rightarrow \pi^*_{\text{TTF}}$	H→L+12 (31%) H-1→L+5 (64%)
		38970	0.10			
	41800	42036	0.11	IA	$\pi_{\text{bzip}} \rightarrow \pi^*_{\text{Mebpy}}$	H-7→L+3/4 (11/10%) H-2→L+4 (25%)
		43016	0.16	ID	$\pi_{\text{TTF}} \rightarrow \pi^*_{\text{TTF}}$	H-5→L+2 (35%)
L²	21600	19304	0.29	ILCT	$\pi_{\text{TTF}} \rightarrow \pi^*_{\text{bzip}}$	H→L (98%)
	29000	28147	0.02	ILCT	$\pi_{\text{TTF}} \rightarrow \pi^*_{\text{bzip}}$	H→L+9 (94%)
	28871	28871	0.05	ID	$\pi_{\text{TTF}} \rightarrow \pi^*_{\text{TTF}}$	H→L+12 (94%)
	30500	29223	0.42	ILCT	$\pi_{\text{TTF}} \rightarrow \pi^*_{\text{bzip}}$	H-1→L (92%)
	32300	32146	0.07	ILCT	$\pi_{\text{TTF}} \rightarrow \pi^*_{\text{bzip}}$	H→L+13 (84%)
	33700	37759	0.24	Ihfac	$\pi_{\text{hfac}} \rightarrow \pi^*_{\text{hfac}}$	H-10→L+2/5 (20/23%) H-9→L+3/4/7 (18/22/70%) H-10→L+6 (22%)
			0.28			
			0.27			
			0.13			
	33900	33736	0.35	ID	$\pi_{\text{TTF}} \rightarrow \pi^*_{\text{TTF}}$	H→L+14 (44%)
	34800	35575	0.28	IA	$\pi_{\text{Mebpy}} \rightarrow \pi^*_{\text{Mebpy}}$	H-11→L+1 (70%)
			0.25			
			0.14			
	36200	36417	0.25	ID	$\pi_{\text{TTF}} \rightarrow \pi^*_{\text{TTF}}$	H-1→L+11 (27%)
		36903	0.14	Ihfac	$\pi_{\text{hfac}} \rightarrow \pi^*_{\text{hfac}}$	H→L+21 (29%) H-8→L+5 (55%)
	40300	/	/	/	/	/

Table S4. Best fitted parameters (χ_T , χ_S , τ and α) with the extended Debye model for compound **3** at 800 Oe in the temperature range 2-10 K.

T / K	χ_T / cm ³ mol ⁻¹	χ_S / cm ³ mol ⁻¹ (fixed)	α	τ / s	R ²
2	24	0.42102	0.51464	12.80799	0.99793
2.2	22.33252	0.3986	0.48938	7.90334	0.99632
2.4	13.74402	0.48205	0.37757	1.40494	0.99453
2.6	10.87475	0.5118	0.29074	0.58464	0.99463
2.8	9.44176	0.50866	0.23088	0.32244	0.99538
3	8.51617	0.49955	0.18879	0.19957	0.99642
3.5	7.09121	0.43864	0.13031	0.07494	0.99809
4	6.1569	0.38913	0.09942	0.03346	0.99895
4.5	5.45447	0.34759	0.08233	0.01676	0.99938
5	4.91075	0.31521	0.0728	0.00921	0.99952
5.5	4.46635	0.29488	0.06537	0.00541	0.99966
6	4.10117	0.28025	0.06566	0.00332	0.99976
7	3.53381	0.27951	0.06864	0.00127	0.99973
8	3.09517	0.32399	0.08094	4.44E-04	0.99982
9	2.75883	0.5769	0.11168	1.83E-04	0.99975
10	2.47995	0.99681	0.07481	1.17E-04	0.99994

Table S5. g tensor and energy splitting for Dy1 and Dy2 in **3**.

	Dy1	Dy2
g tensor		
g_x	0.014	0.003
g_y	0.027	0.008
g_z	19.240	19.341
Energy splitting (cm ⁻¹)		
1	0	0
2	99.1	92.6
3	115.1	114.9
4	152.1	150.5
5	175.3	178.3
6	199.7	193.7
7	257.4	237.2
8	431.1	436.0